https://doi.org/10.5194/egusphere-2025-5971
Preprint. Discussion started: 19 January 2026

Top-down estimate of regional carbon sinks over East Asia for 2010–2019 using satellite observations

Mina Kim[1], Rokjin J. Park[1*], Jingi Jung[1], Sang-Ik Oh[1], Eunjo S. Ha[1], Jaein I. Jeong[1], Sang-Wook Yeh[2]

[1]School of Earth and Environmental Science, Seoul National University, Seoul, Republic of Korea
[2]Department of Marine Sciences and Convergent Engineering, Hanyang University, ERICA, Republic of Korea

Correspondence to: Rokjin J. Park (rjpark@snu.ac.kr)

Abstract. East Asia is a major source of fossil fuel emissions and strongly influences regional and global CO_2 concentrations. Quantifying natural carbon sinks in this region is therefore essential for improving climate projections and informing mitigation strategies. We estimated the Net Ecosystem Exchange (NEE) and ocean carbon fluxes over East Asia (18.5°N–54°N, 73°E–146°E) during 2010–2019 using a Bayesian inversion framework. The GEOS-Chem chemical transport model was combined with GOSAT ACOS v9.0 XCO_2 retrievals, and region-specific prior uncertainties were assigned using standard deviations from land and ocean models. Posterior estimates show enhanced carbon uptake relative to the prior, with NEE increasing from -0.17 ± 0.08 to -0.31 ± 0.06 PgC yr^{-1} and ocean uptake changing slightly from -0.20 ± 0.03 to -0.21 ± 0.03 PgC yr^{-1}. Simulated CO_2 concentrations based on posterior fluxes agreed better with independent observations than those from prior fluxes. Most subregions in East Asia acted as net carbon sinks over the past decade. Enhanced Vegetation Index (EVI) trends also support strengthened carbon uptake. However, several regions showed temporary net carbon releases in 2015–2016, likely linked to the strong 2015/16 El Niño. East Asia released a net flux of +3.45 PgC yr^{-1} to the atmosphere during 2010–2019. Natural sinks offset only ~13.6% of fossil fuel emissions, leaving a substantial residual source. Despite strengthened posterior sinks, they remain insufficient to counter regional emissions, sustaining elevated CO_2 levels and continued outflow from East Asia.

1 Introduction

Carbon dioxide (CO_2) is the most important anthropogenic greenhouse gas (GHG), with atmospheric concentrations having risen from the pre-industrial level of 280 ppm to 426 ppm in 2025 (Joos and Spahni, 2008; Lan et al., 2025). To achieve the Paris Agreement's goal of limiting global temperature rise to below 1.5 °C above pre-industrial levels (UNFCCC, 2015), effective carbon management is imperative. This entails not only controlling anthropogenic emissions but also improving our understanding of carbon sink mechanisms, as major natural sinks such as vegetation and oceans currently absorb roughly half of global emissions (Friedlingstein et al., 2023). However, significant uncertainties remain regarding the capacity and dynamics of these natural sinks (IPCC, 2023). This problem is particularly acute in East Asia, one of the world's fastest-growing carbon-emitting regions (Gilfillan and Marland, 2021). Despite its critical role, previous studies have struggled to

https://doi.org/10.5194/egusphere-2025-5971
Preprint. Discussion started: 19 January 2026

accurately estimate regional carbon flux due to the limited number of in situ CO_2 observation sites in Asia compared to Europe or North America (Park and Kim, 2020), which poses a limitation to the accuracy of inverse modeling and regional flux estimates.

Carbon fluxes are commonly estimated using two main approaches: top-down and bottom-up. Top-down methods infer surface fluxes by applying inverse techniques to atmospheric CO_2 concentration data, whereas bottom-up methods combine observations with statistical upscaling or process-based models (Jung et al., 2020; Kondo et al., 2020; Sitch et al., 2008, 2015). Among top-down techniques, atmospheric inversions driven by a chemical transport model (CTM) are widely used (Basu et al., 2018; Nassar et al., 2011; Palmer et al., 2003; Peylin et al., 2013).

Since in situ CO_2 measurements are highly precise (typical observational errors <0.2 ppm), they have been extensively used in inversion frameworks (Baker et al., 2006; Deng and Chen, 2011; Gurney et al., 2003; Jiang et al., 2013; Monteil et al., 2020; Peylin et al., 2013). Their major limitation is sparse spatial coverage, especially over data-poor regions such as the oceans and much of Africa. Satellite retrievals, by contrast, provide broad spatial coverage: for example, GOSAT has a footprint approximately 10.5 km in diameter with an observation error of about 1 ppm (Kulawik et al., 2019). Whereas Wang et al. (2019) excluded oceanic soundings because of larger uncertainties associated with glint-mode retrievals(Wunch et al., 2017), the present study adopts a different strategy. We use both land and ocean observations and explicitly account for the instrument error reported in the GOSAT product. By weighting each sounding by its stated uncertainty, we retain more measurements while limiting the influence of noisier data, thereby improving spatial coverage for flux estimation.

Although many studies have targeted East Asia, most focus on China and provide limited quantitative assessment of flux uncertainties. For example, Wang et al. (2020) estimated Chinese carbon fluxes from in situ data, assigning prior uncertainties of 50% for land and 40% for ocean, which were prescribed as simple percentage values rather than derived from data variability. Thompson et al. (2016) used a seven-model inversion ensemble for Asia, but applied inconsistent prior fluxes and uncertainties across models. Jiang et al. (2013) estimated carbon uptake in China using ground observations. In their framework, land prior uncertainties were derived from net primary production, while a uniform prior uncertainty was assumed for the ocean.

Here, we explicitly treat uncertainties in both terrestrial and oceanic fluxes. Terrestrial uncertainties are derived from the standard deviation of the TRENDY ensemble (Sitch et al., 2015), and ocean flux uncertainties are based on the standard deviation among ocean models contributing to the Global Carbon Project (Friedlingstein et al., 2023). Given the central role of error specification in inverse modeling, this data-informed approach yields a more consistent quantification of prior uncertainties and enhances the robustness of posterior flux estimates. Using this framework, we estimate East Asian carbon fluxes from GOSAT XCO_2 retrievals and introduce an uncertainty structure that varies by region and domain (land/ocean). These refinements aim to provide a more accurate assessment of regional carbon fluxes than previous studies, supporting evidence-based policymaking and climate-mitigation strategies.

https://doi.org/10.5194/egusphere-2025-5971
Preprint. Discussion started: 19 January 2026

2 Data and methods

2.1 Forward model

We used GEOS-Chem v13.1.0 as a forward model to relate atmospheric CO_2 concentrations to surface fluxes for optimization in the inverse modeling framework. GEOS-Chem is a global 3D chemical transport model driven by meteorological inputs from the Goddard Earth Observing System (GEOS) of NASA's Global Modeling and Assimilation Office (GMAO). The CO_2 simulation in GEOS-Chem was originally developed by Suntharalingam et al. (2004) and later updated by Nassar et al., (2010, 2013). For high-resolution CO_2 simulations over East Asia, we used the nested-grid version of GEOS-Chem, which is driven by MERRA-2 meteorological data with a 0.5° × 0.625° horizontal resolution and 47 vertical levels from the surface to 0.01 hPa. The simulation domain covers East Asia (18.5°N–54°N, 73°E–146°E), with boundary conditions derived from the global 2° × 2.5° simulation.

The model used monthly anthropogenic CO_2 emissions from the Open-source Data Inventory for Anthropogenic CO_2 (ODIAC2020b; Oda and Maksyutov, 2011; Oda et al., 2018) and weekly biomass burning emissions derived from the Global Fire Emissions Database version 4.1 (GFEDv4; Randerson et al., 2018). The model also includes CO_2 emissions from shipping and aviation, as well as chemical production from the oxidation of carbon monoxide (CO), methane (CH_4), and non-methane volatile organic compounds (NMVOCs). The model simulates CO_2 sinks as a first-order process using monthly NEE from the Dynamic Land Ecosystem Model (DLEM; Tian et al., 2010; You et al., 2022) and monthly ocean CO_2 fluxes from the Finite-Element Sea ice–Ocean Model coupled with the Regulated Ecosystem Model (FESOM-REcoM; Schourup-Kristensen et al., 2018).

Our study focused on optimizing NEE and ocean exchange fluxes. Following common practice in inverse modeling, we assumed no errors in fossil fuel and biomass burning fluxes (e.g., Chevallier et al., 2019; Gurney et al., 2002; Peters et al., 2007). To optimize fluxes consistent with administrative boundaries, we performed tagged CO_2 simulations that allowed us to independently track CO_2 originating from each region (Figure 1). These defined regions comprise the Korean Peninsula, China, Mongolia, Taiwan, Japan, and parts of the Northwest Pacific. After a five-year spin-up starting from January 2005, the model simulations were conducted from January 2010 to December 2019 to incorporate GOSAT observations, which became available starting in 2009.

https://doi.org/10.5194/egusphere-2025-5971
Preprint. Discussion started: 19 January 2026

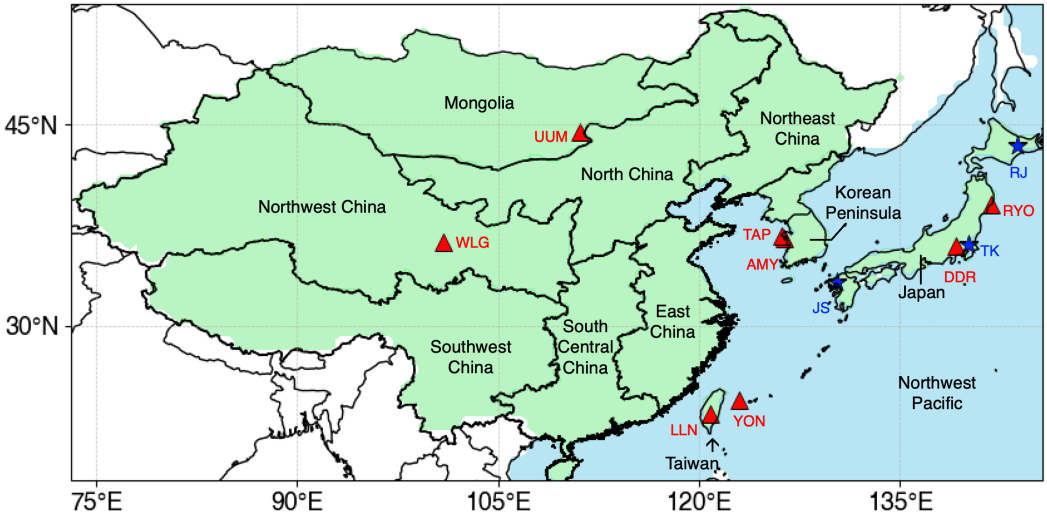

Figure 1. Spatial domains defined in this study for regional analysis over East Asia (18.5°N–54°N, 73°E–146°E), including Mongolia, China (six subregions), the Korean Peninsula, Japan, Taiwan, and the Northwest Pacific. Red triangles indicate surface CO2 observation sites from the WDCGG network, and blue stars represent TCCON stations.

2.1 Inverse model

To infer surface fluxes from atmospheric CO_2 concentrations, we employ an inverse modeling framework based on optimal estimation theory (Rodgers, 2000). Observed concentrations of CO_2, assembled into an observation vector y, are related to the sources and sinks of CO_2 (assembled in a state vector x) through the Jacobian matrix **K**, as described by the following equation:

$$y = Kx + \varepsilon \quad (1)$$

The Jacobian matrix **K** represents the forward model introduced in the previous section. Under the linear approximation, it links variations in the state vector to corresponding changes in the modeled concentrations. The state vector x represents the annual sink/source originating from vegetation and the ocean, while the observation vector y is defined by GOSAT XCO_2 (Sect. 2.3). The error vector ε includes contributions from measurement accuracy, representation error, and errors in model parameters. The ensemble characteristics of these errors are described by the observation error covariance (S_o), which is represented as the sum of the covariance matrices from individual sources of error.

The fundamental principle of an optimal estimation inverse method is to minimize a cost function $J(x)$:

$$J(x) = (y - Kx)^T S_o^{-1}(y - Kx) + (x - x_a)^T S_a^{-1}(x - x_a) \quad (2)$$

where x_a is the a priori state vector and S_a is the error covariance matrix for the a priori state vector (x_a). The optimized a posteriori state vector ($\hat{x}$) is given as follows:

https://doi.org/10.5194/egusphere-2025-5971
Preprint. Discussion started: 19 January 2026

$$\hat{x} = x_a + (K^T S_o^{-1} K + S_a)^{-1} K^T S_o^{-1} (y - K x_a) \quad (3)$$

The superscript **T** indicates the matrix transpose. The a posteriori error covariance matrix $\hat{S}$, which describes the uncertainty of the optimized state estimate, is given by the following expression.

$$\hat{S} = (K^T S_o^{-1} K + S_a^{-1})^{-1} \quad (4)$$

2.3 Error specification

2.3.1 A priori error covariance (S_a)

The a priori error covariance matrix (S_a) is constructed with the squares of the a priori uncertainties (σ_a) as its diagonal elements. In this study, the σ_a values for terrestrial fluxes are derived from the standard deviation of NEE across eight land models (CABLE-POP, CARDAMOM, CLASSIC, DLEM, EDv3, IBIS, OCN, and YIBS) participating in the Trends in Net Land-Atmosphere Carbon Exchange (TRENDY) project (Sitch et al., 2008). TRENDY is an ensemble of terrestrial biosphere models forced by common meteorological inputs. Similarly, the σ_a values for ocean fluxes are defined using the standard deviation from a ten-model ocean ensemble (ACCESS, CESM, CNRM, FESOM, IPSL, MOM, MPIOM, MRI, NEMO, and NORESM) contributing to the Global Carbon Budget project (Friedlingstein et al., 2023). The resulting annual σ_a values for each region are summarized in Table 1.

Only a few previous inversion studies have implemented time-varying prior uncertainties at seasonal or monthly scales (e.g., Baker et al., 2006). However, allowing σ_a to vary interannually provides a more consistent representation of how flux uncertainty evolves in response to climate variability. This configuration enables the inversion to account for year-to-year changes in terrestrial and oceanic fluxes, rather than relying on a stationary error structure. In our sensitivity test, time-invariant uncertainties produced regional flux differences that averaged about 12.4% relative to the time-varying case. While this sensitivity analysis does not by itself demonstrate that the time-varying configuration is more realistic, it indicates that allowing σ_a to vary in time can have a non-negligible influence on the inferred regional fluxes.

Table 1. Annual a priori uncertainty (σ_a) for regional fluxes (TgC yr^{-1}). The values are derived from the standard deviation across TRENDY biosphere models (Sitch et al., 2008)**, except for the Northwest Pacific region, which is estimated from the ocean model ensemble contributing to the Global Carbon Budget** (Friedlingstein et al., 2023)**.**

Year	Korean peninsula	Japan	North China	North east China	East China	South Central China	South west China	North west China	Mongolia	Taiwan	North west Pacific
2010	8.7	13.0	22.8	30.1	43.7	38.6	52.1	16.5	12.4	1.3	33.0
2011	6.8	10.2	23.7	17.2	36.3	51.2	34.7	15.0	13.9	1.1	30.8
2012	10.3	10.3	35.7	23.5	35.8	33.4	46.3	14.3	32.1	1.3	31.9

https://doi.org/10.5194/egusphere-2025-5971
Preprint. Discussion started: 19 January 2026

2013	8.7	7.9	32.2	18.1	34.8	28.9	46.8	22.4	36.7	1.1	31.5
2014	9.2	8.3	28.1	21.0	38.0	31.8	28.3	12.6	26.9	1.0	31.6
2015	8.6	12.4	28.2	23.7	37.1	35.4	30.2	23.4	29.1	1.2	27.4
2016	6.0	9.2	31.1	26.7	45.3	36.4	29.6	31.6	15.5	0.9	26.0
2017	9.1	6.5	36.2	31.8	34.5	23.0	23.1	19.0	18.5	1.0	30.4
2018	5.8	14.9	29.7	24.1	40.4	36.9	33.9	18.0	29.6	1.3	30.9
2019	5.4	8.7	31.3	19.4	55.4	48.2	45.7	16.0	25.8	1.3	27.4
Mean	7.8	10.1	29.9	23.6	40.1	36.4	37.1	18.9	24.0	1.2	30.1

2.3.2 Observational error covariance (S_o)

The total observation error covariance, S_o includes contributions from forward model (CTM) error, representation error, and instrument error ($S_o = S_M + S_R + S_I$). The forward model errors are estimated from the relative residual standard deviation (RRSD) of the difference between the model and observation, as represented by ($\mathbf{K}x-y$)/y (Palmer et al., 2003). It is assumed that the mean model bias arises from errors in the a priori sources, and that the variance reflects uncertainty associated with the model. Representation errors are assigned as 1% of the observed concentration (approximately 4 ppm), consistent with the magnitude reported in previous studies. Kaminski et al. (2010) used an ad hoc variability of 3 ppm, Gerbig et al. (2003) reported representation errors of similar magnitude (~3 ppm), and Tolk et al. (2008) recommended values of around 3 ppm depending on model resolution.

2.4 Observations

GOSAT is a greenhouse gas observation satellite launched in February 2009, operating in a sun-synchronous orbit. Compared to OCO-2, which was launched in 2015, GOSAT has a longer period of available data, making it commonly used in top-down emission estimation studies (Jiang et al., 2022; Byrne et al., 2019; Liu et al., 2021; Houweling et al., 2015). GOSAT provides column-averaged dry-air mole fractions of CO_2, referred to as XCO_2.

We use the Atmospheric CO_2 Observations from Space (ACOS) Version 9.0 Level 2 Lite product (Taylor et al., 2022), covering the period from January 2010 to December 2019. This dataset includes bias correction, with a global mean bias of less than 0.2 ppm (Taylor et al., 2022). It has a spatial resolution of 10.5 km × 10.5 km at nadir and is regridded to 2° × 2.5° (Global) or 0.5° × 0.625° (East Asia) to match GEOS-Chem resolution. To ensure data reliability, only retrievals with a quality flag of zero were used, where a value of 0 denotes "good" quality and a value of 1 denotes "bad" quality. The XCO_2 uncertainty was used to construct the observational error covariance (Section 2.3.2). The averaging kernel, pressure weighting function, and a priori profile are used to construct the transformed model XCO_2, incorporating observational sensitivity based on Eq. (5) (Connor et al., 2008).

https://doi.org/10.5194/egusphere-2025-5971
Preprint. Discussion started: 19 January 2026

$$XCO_2^m = XCO_2^a + \sum_j h_j \, a_{CO_2,j} (x_m - x_a)_j \quad (5)$$

Here, XCO_2^m is transformed model XCO_2, and XCO_2^a is the a priori XCO_2 from GOSAT/ACOS Version 9.0 Level 2 Lite product. h_j is the pressure weighting function and $a_{CO_2,j}$ is the column averaging kernel of GOSAT/ACOS v9r. x_m represents the model-simulated vertical CO_2 profile, and x_a is the a priori CO_2 profile from GOSAT/ACOS v9r.

We used independent ground-based observations to validate our estimates of CO_2 fluxes in the model. They include World Data Centre for Greenhouse Gases (WDCGG), operated by the Japan Meteorological Agency (JMA) under the Global Atmosphere Watch (GAW) program of the World Meteorological Organization (WMO), provides high-precision CO_2 concentration data from ground-based stations worldwide. These observations undergo rigorous calibration and quality control procedures, making them highly suitable as an independent benchmark for evaluating model performance. Within the study domain (18.5°N–54°N, 73°E–146°E), a total of eight WDCGG stations with sufficient temporal coverage were identified after applying the RMSE-based filtering criterion described in Section 3. The locations of the WDCGG stations are shown in Figure 1 (red triangles).

Total Carbon Column Observing Network (TCCON; Wunch et al., 2011) provides ground-based measurements of column-averaged CO_2 concentrations (XCO_2) using Fourier transform spectrometers. In this study, we used the GGG2020 product, which includes a priori CO_2 vertical profiles necessary for generating modeled XCO_2 from atmospheric transport models. Within the spatial domain of this study and over the relevant time period, three TCCON sites were available for evaluation. The locations of the TCCON stations are shown in Figure 1 (blue stars).

3 Evaluation (a priori vs. a posteriori)

To evaluate the reliability of the inversion results, we compared the simulated CO_2 concentrations from both the prior and posterior flux with independent observational datasets, namely WDCGG and TCCON, which were not assimilated into the inversion system (Feng et al., 2020; Jiang et al., 2021; Jin et al., 2018; Wang et al., 2019). This approach allows for an objective assessment of the inversion performance.

Three statistical metrics were employed for the evaluation: correlation coefficient (R), root mean square error (RMSE), and normalized mean bias (NMB), which quantify the linear relationship, overall error magnitude, and systematic bias between the modeled and observed CO_2 concentrations, respectively.

To ensure that the evaluation reflects large-scale, well-mixed CO_2 variability rather than local influences or large representation errors, sites with model–observation RMSE exceeding 7.0 ppm were excluded. This threshold approximately corresponds to the annual amplitude of the seasonal cycle at Mauna Loa, a globally representative background site. Errors exceeding this threshold suggest that the station is influenced by sub-grid variability that GEOS-Chem cannot resolve at its native resolution, making such sites unsuitable for model evaluation. Following the approach of Jiang et al. (2022), which

https://doi.org/10.5194/egusphere-2025-5971
Preprint. Discussion started: 19 January 2026

excluded sites with inadequate model performance, we removed three WDCGG stations (KIS, HKG, and HKO), representing Kisai (Japan), Hong Kong Hok Tsui (China), and Hong Kong King's Park (China). All TCCON stations met the performance criterion and were retained.

We evaluated the inversion results using eight WDCGG and three TCCON observation sites (Sect. 2.4). Since WDCGG provides point-based ground-level measurements, we selected the nearest model grid cell based on the latitude, longitude, and altitude of each observation site for comparison. Among the WDCGG sites, all except YON showed improvements in all three statistical metrics, correlation coefficient (R), root mean square error (RMSE), and normalized mean bias (NMB), after the inversion (Table 2). The YON site, located at the southernmost edge of the domain, lies on a small island (~28.9 km^2), which likely introduced substantial represent errors due to the mismatch with the coarser model resolution. For the TCCON observations, which represent column-averaged CO_2 concentrations, we computed the modeled XCO_2 using Eq. (5) to ensure a consistent comparison. All three TCCON sites showed improvements across all evaluation metrics.

The posterior simulation improved the overall model performance, reducing the mean RMSE from 3.08 to 2.94 ppm and the mean NMB from 0.33 % to 0.28 %, while maintaining a high correlation (R = 0.95). Although the overall improvements were moderate, they represent consistent enhancements at 10 of the 11 sites and are statistically significant. A paired t-test across all WDCGG and TCCON sites confirmed significant improvements after the inversion: the correlation coefficient increased ($\Delta R = +0.005$, $p = 0.012$), the normalized mean bias decreased ($\Delta NMB = -0.03$ %, $p = 0.037$), and the RMSE decreased by 0.15 ppm on average ($p = 0.006$). Furthermore, both overestimations (positive NMB at most sites) and underestimations (negative NMB at LLN and TAP) were reduced after optimization, suggesting that the improvement was not coincidental but systematic. A moderate level of improvement, which is commonly reported in CO_2 inversion studies, arises because CO_2 fields are already well constrained by the background state, while the remaining discrepancies are primarily attributed to transport and representation errors. For instance, Kou et al. (2023) reported only marginal improvements (RMSE: 2.65 → 2.63 ppm; R: 0.66 → 0.66; MAE: 2.03 → 2.02 ppm), emphasizing that such modest statistical changes are typical in atmospheric CO_2 inversions.

Table 2. Evaluation metrics for prior and posterior CO_2 concentrations using ground-based observations

Observation	R		NMB (%)		RMSE (ppm)	
	Prior	Posterior	Prior	Posterior	Prior	Posterior
WDCGG						
AMY	0.95	0.95	1.27	1.21	5.87	5.54
DDR	0.95	0.96	0.57	0.51	0.57	0.51
LLN	0.97	0.97	-0.34	-0.33	3.01	2.99
RYO	0.95	0.96	0.49	0.43	3.31	3.03
TAP	0.92	0.93	-0.85	-0.79	4.85	4.59

https://doi.org/10.5194/egusphere-2025-5971
Preprint. Discussion started: 19 January 2026

UUM	0.92	0.93	0.35	0.28	3.61	3.41
WLG	0.95	0.96	0.26	0.18	2.6	2.29
YON	0.99	0.99	0.11	0.13	1.1	1.22
TCCON						
JS	0.97	0.97	0.44	0.43	2.34	2.26
RJ	0.92	0.92	0.70	0.70	3.58	3.56
TK	0.93	0.93	0.61	0.59	2.99	2.87

Uncertainty Reduction (UR) is a key metric for evaluating the performance of inverse modeling, as it quantifies the reduction in prior uncertainty (Deng et al., 2007). It is defined as :

$$UR = \left(1 - \frac{\sigma_{posterior}}{\sigma_{prior}}\right) \times 100 \quad (6)$$

The UR in China is relatively high, likely due to its large spatial extent, which allows for the inclusion of a greater number of GOSAT XCO_2 pixels, indicating that it is more effectively constrained. In contrast, Taiwan, being much smaller in size, includes relatively fewer GOSAT XCO_2 pixels, resulting in a weaker constraint. UR of regional carbon flux estimates varies substantially across time and space (Deng et al., 2014; Takagi et al., 2011). Over ocean regions, the UR is lower than over land, primarily due to the limited spatial coverage of GOSAT over the ocean and the higher uncertainty associated with satellite observations in these areas (Wunch et al., 2017). This spatial pattern is consistent with the findings of Deng et al. (2014), who demonstrated that UR is closely related to the spatial coverage of GOSAT XCO_2 observations. Similarly, Jiang et al. (2021) reported that UR over land ranged from 5.9% to 27.2%, whereas ocean UR remained relatively low, ranging from 0.12% to 3.7%. Such large spatial variations in UR highlight its strong dependence on observational density. These results suggest that dense and spatially extensive observational coverage is essential for achieving a stronger constraint on regional carbon fluxes.

Table 3. Mean uncertainty reduction rate (UR) for each region for the period 2010-2019

Region	UR (%)
Korean peninsula	3.80
Japan	8.91
North China	41.14
Northeast China	57.02
East China	35.50

https://doi.org/10.5194/egusphere-2025-5971
Preprint. Discussion started: 19 January 2026

South Central China	36.36
Southwest China	28.84
Northwest China	20.74
Mongolia	21.67
Taiwan	0.00
Northwest Pacific	0.66

4 Regional a posteriori CO2 flux and its annual variability

This section describes regional changes in prior and posterior estimates of carbon fluxes. The 10-year mean NEE increased from –0.17 ± 0.08 PgC yr^{-1} to –0.31 ± 0.06 PgC yr^{-1} (Figure 2a, b), while oceanic uptake showed a slight increase from –0.20 ± 0.03 PgC yr^{-1} to –0.21 ± 0.03 PgC yr^{-1}, although this change lies within the range of prior uncertainty and is therefore not statistically significant (Figure 2a, b). Most regions exhibited a trend toward enhanced carbon uptake, as shown in the difference map (Figure 2c).

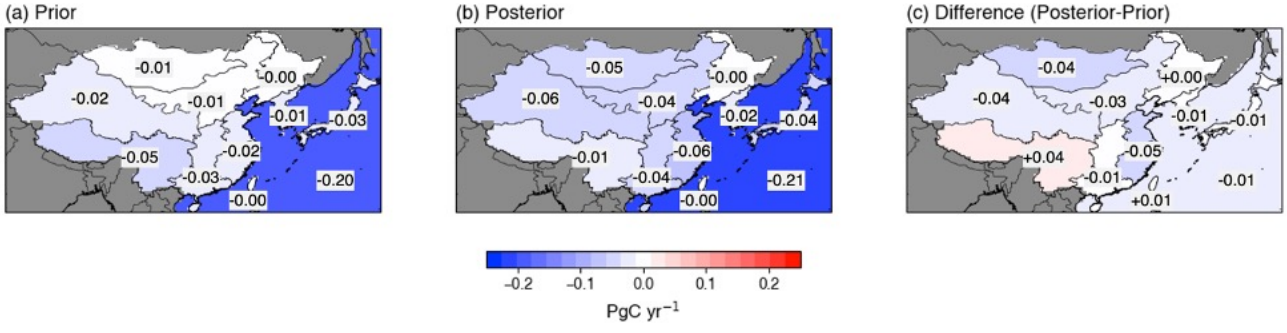

Figure 2. Regional carbon fluxes over East Asia averaged for the period 2010–2019 from (a) the prior estimate, (b) the posterior estimate, and (c) their difference (posterior − prior). Negative values indicate net carbon uptake (sink), and positive values indicate net carbon emissions (source).

In particular, Mongolia, characterized by its vast grasslands, initially showed very weak carbon uptake of –0.01 PgC yr^{-1} in the prior estimate, which increased to –0.05 PgC yr^{-1} in the posterior. Most regions in China experienced increases in carbon uptake, although the magnitude of enhancement varied across subregions. In contrast, carbon uptake weakened in Southwest China, while Northeast China remained nearly neutral with little change from the prior estimate. On the Korean

https://doi.org/10.5194/egusphere-2025-5971
Preprint. Discussion started: 19 January 2026

Peninsula, carbon uptake increased, and Japan exhibited a similar level of enhancement. Taiwan, however, showed little to no change. Oceanic regions showed no substantial change.

Terrestrial carbon uptake responds non-linearly to complex environmental drivers such as drought and El Niño events (Yue et al., 2017). As a result, vegetation indices cannot perfectly represent variations in carbon fluxes. Despite these limitations, carbon uptake remains fundamentally linked to photosynthetic activity, and the Enhanced Vegetation Index (EVI) provides one of the most practical and widely used proxies for photosynthesis by reflecting vegetation greenness. (Noumonvi and Ferlan, 2020) also demonstrated that EVI serves as one of the best satellite-based indicators of NEE, even though it cannot fully capture respiration-related processes or short-term environmental stress. Previous studies (e.g., Wang et al., 2020; Jiang et al., 2021) have used satellite-derived vegetation indices such as EVI, NDVI, and LAI to estimate carbon fluxes. These analyses were generally conducted at coarse spatial scales, typically at continental or subcontinental levels, without resolving fine-scale regional heterogeneity. Following this approach, our comparison also focuses on the domain-averaged behavior. Figure 3 presents the time series of domain-averaged EVI with seasonal variations removed. This increasing trend in EVI suggests enhanced vegetation activity, supporting our finding of increased carbon uptake across most regions of East Asia. Similarly, Wang et al. (2020) attributed China's substantial carbon uptake to the annual rise in vegetation indices.

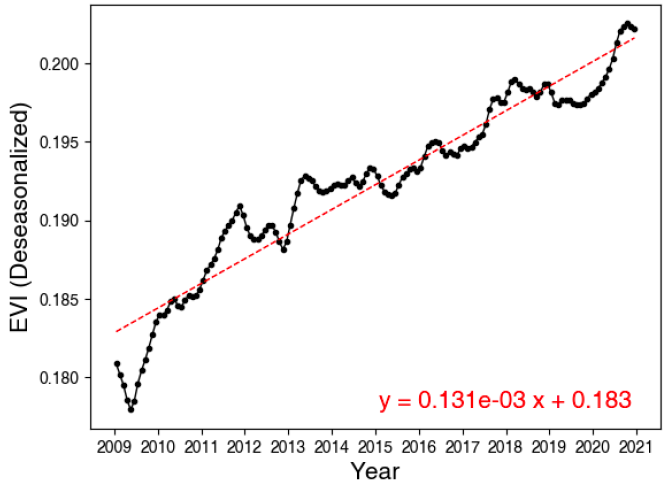

Figure 3. Time series of the domain-averaged Enhanced Vegetation Index (EVI) after removing seasonality. The red dashed line indicates the linear trend fitted to the deseasonalized EVI values.

We examine regional interannual variability and associated supporting evidence, such as ENSO and EVI, that may help explain observed flux patterns. Notably, 2015–2016 coincided with one of the three strongest Super El Niño events on record (1982–83, 1997–98, and 2015–16; Ren et al., 2017; WMO, 2017). ENSO (El Niño–Southern Oscillation) is known to influence photosynthesis and carbon uptake by altering temperature and precipitation patterns (Cox et al., 2013; Fang et al.,

https://doi.org/10.5194/egusphere-2025-5971
Preprint. Discussion started: 19 January 2026

2017; Wang et al., 2013; Wang et al., 2014). Accordingly, we focus on ENSO-related impacts, and extend the analysis of EVI by conducting correlation analyses to assess its temporal relationship with fluxes.

Figure 4 presents annual CO_2 fluxes for all regions considered in this study over 2010–2019, allowing for direct comparison of prior and posterior estimates across East Asia. The Korean Peninsula acted as a weak carbon sink with low interannual variability. For all years, posterior estimates consistently showed stronger uptake than prior estimates. Japan exhibited a similar pattern, with posterior values exceeding prior ones, and overall low variability. In Mongolia, prior estimates indicated a weak sink, while posterior estimates showed markedly enhanced uptake. Except for 2017, which showed a shift toward a weak source, all years suggested a sink. In Taiwan, posterior fluxes were comparable to or slightly lower than the prior, and overall fluxes remained relatively stable. Notably, both prior and posterior estimates indicated decreased carbon uptake during 2015–2016, coinciding with the Super El Niño. Bastos et al. (2018) reported that this event substantially reduced terrestrial carbon uptake globally by suppressing ecosystem productivity, within our study domain the influence of El Niño was mainly concentrated over China, where several studies (Ma et al., 2018; Zhai et al., 2016) consistently reported a characteristic south-flood north-drought pattern (Zhai et al., 2016).

In northern China (North, Northwest, and Northeast China), precipitation deficits prevailed during the 2015 El Niño peak, especially in North China, where severe summer droughts were reported (Zhai et al., 2016), followed by near-normal or slightly wetter conditions in 2016 (Ma et al., 2018). These anomalies are consistent with our results, which indicate a transition from carbon release in 2015 (0.008 PgC yr^{-1}) to weak carbon uptake in 2016 (−0.005 PgC yr^{-1}; Figure 4). In Northwest China, by contrast, the residual effects of the 2015–2016 El Niño brought unusually high rainfall during 2016 (Lu et al., 2019), particularly in spring and autumn, when precipitation exceeded 150% of the climatological mean (Ma et al., 2018). As noted by Liu et al. (2024), vegetation in arid regions tends to respond positively to increased moisture availability, and our posterior flux estimates indeed indicate sustained or even enhanced carbon uptake during this period. Specifically, the mean flux during 2015–2016 (−0.078 PgC yr^{-1}) was more negative than the decadal mean excluding those years (−0.054 PgC yr^{-1}), suggesting strengthened carbon uptake under wetter conditions. In Northeast China, interannual flux variability was large, with strong uptake in 2016, but the statistical correlation with ENSO remained insignificant ($p > 0.05$; Ma et al., 2018). This region encompasses diverse vegetation types and spans arid to humid zones (see Jiang et al., 2022; Fig. 1b), potentially explaining its high interannual flux variability.

In southern China (East, South Central, and Southwest China), the El Niño–induced precipitation anomalies were generally opposite to those in the northern China. However, Southwest China represented an exception. While East and South Central China experienced excessive rainfall and flooding, Southwest China underwent persistent drought due to weakened southward moisture transport (Ma et al., 2018). This region suffered from prolonged drought conditions from summer 2015 through spring 2016, leading to vegetation water stress and reduced carbon uptake, with net carbon emissions of 0.011 and 0.023 PgC yr^{-1} during these two years. In contrast, the summer 2016 flood East China was particularly severe. The WMO reported that flooding across the Yangtze River Basin in summer 2016 was the most serious since 1999 (WMO, 2017). This extreme rainfall event coincided with a marked shift toward positive NEE (+0.092; carbon release) in 2016 (Figure 4). South

https://doi.org/10.5194/egusphere-2025-5971
Preprint. Discussion started: 19 January 2026

Central China similarly exhibited enhanced precipitation and frequent flooding during 2015–2016 (Ma et al., 2018), corresponding to nearly neutral and carbon-releasing conditions in those years (−0.001 and +0.011 PgC yr^{-1}).

While numerous studies have addressed the effects of ENSO on temperature, precipitation, and extreme weather events, few have explored its direct influence on regional carbon fluxes. Our analysis provides new evidence that ENSO-related climatic variability also affects vegetation carbon uptake across East Asia, thereby contributing to bridging this critical research gap.

We also analyzed the correlations between EVI and carbon uptake (defined as the negative of NEE, so that positive values indicate uptake). Overall, the correlations strengthened across most regions (Table 4), particularly in the northern part of the domain, including Northwest China, Korean Peninsula, and Japan. For example, the correlation coefficients increased from 0.60 → 0.75 in Korean Peninsula**,** 0.55 → 0.69 in Japan**,** and 0.09 → 0.78 in Northwest China**,** respectively. In North and Northeast China and Mongolia, the correlations shifted from negative to positive, while East China showed a slight increase.

However, it is unrealistic to expect consistent improvement in vegetation–carbon correlations across all regions. For reference, Jiang et al. (2021) compared the relationships between carbon sinks and two vegetation-related indicators (SDA and LAI; their Table 5) and reported correlation improvements in fewer than half of the regions examined. In our study, correlations weakened in South Central and Southwest China, and in Taiwan the negative correlation persisted. These southern regions are dominated by evergreen broad-leaved forests (Zhu and Tan, 2024). According to Buchmann and Schulze (1999), broad-leaved forests differ from other ecosystems in that leaf area index (LAI) does not significantly correlate with carbon uptake, due to self-shading and increased ecosystem respiration that offset photosynthetic gains. Although EVI differs from LAI, Potithep et al. (2013) reported a high correlation between the two in broad-leaved forests ($r^2 = 0.96$), suggesting a close relationship. This may explain why EVI–carbon uptake correlations did not improve in South and Southwest China and Taiwan, where broad-leaved forest characteristics dominate.

https://doi.org/10.5194/egusphere-2025-5971
Preprint. Discussion started: 19 January 2026

335

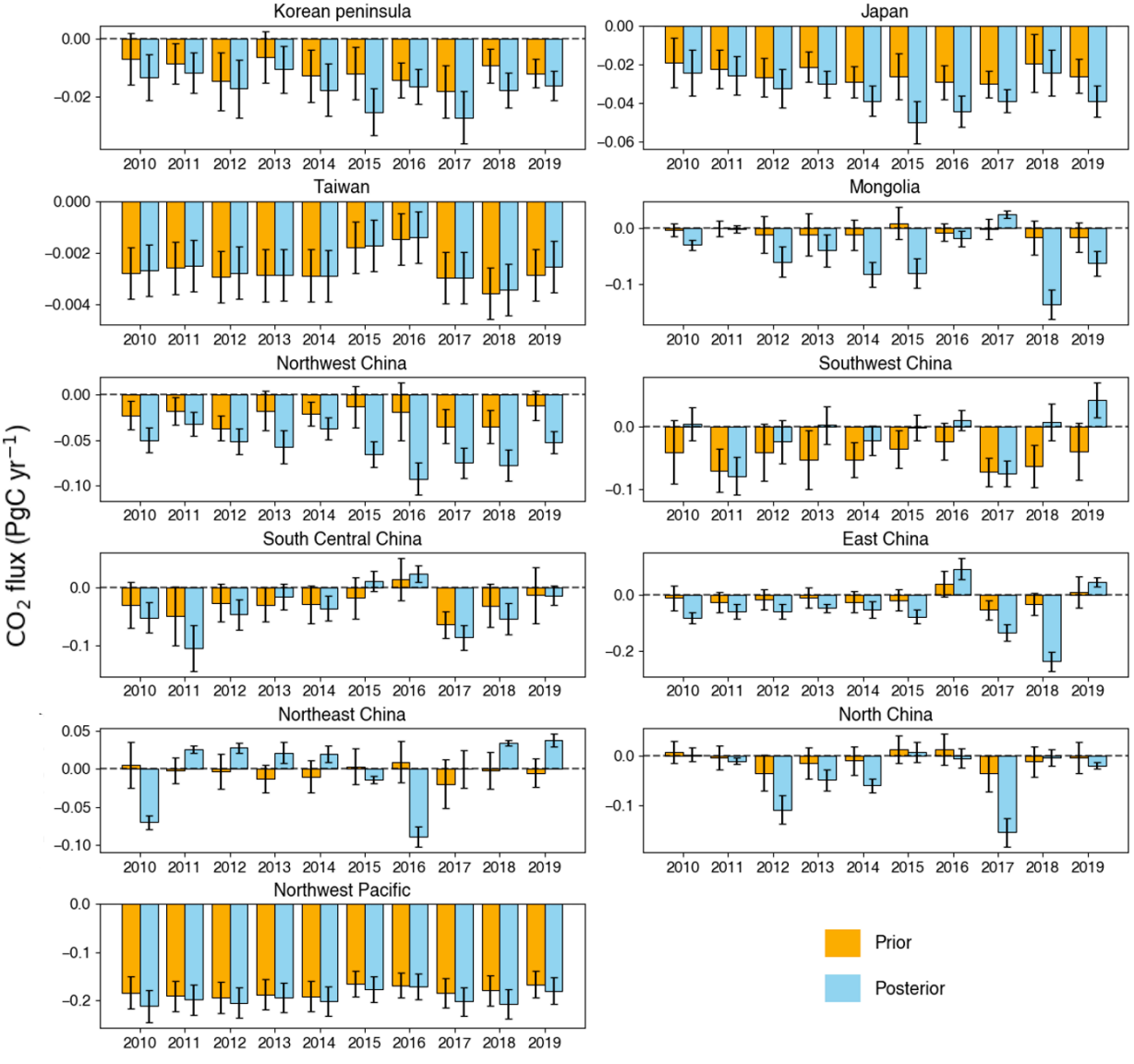

Figure 4. Annual regional CO_2 fluxes over East Asia for the period 2010–2019, estimated from the prior (orange) and posterior (blue) fluxes. Each panel represents a different region, and negative values indicate net CO_2 uptake (sink). Error bars represent the uncertainty of the flux estimates.

340

https://doi.org/10.5194/egusphere-2025-5971
Preprint. Discussion started: 19 January 2026

Table 4. Correlation coefficients between Enhanced Vegetation Index (EVI) and regional vegetation CO_2 uptake, represented as negative NEE.

Region	Correlation coefficient with EVI	
	Prior	Posterior
Korean peninsula	0.60	0.75
Japan	0.55	0.69
North China	−0.13	0.07
Northeast China	−0.01	0.32
East China	0.04	0.13
South Central China	−0.21	−0.39
Southwest China	−0.03	−0.08
Northwest China	0.09	0.78
Mongolia	−0.13	0.06
Taiwan	−0.24	−0.22

5. Comparison with other top-down and bottom-up product

In this study, we evaluate the characteristics and discrepancies of our posterior carbon flux estimates by comparing them with a suite of established products derived from diverse estimation frameworks. The comparison encompasses FLUXCOM (NEE and ocean), GCAS2021 (NEE), TRENDY (NEE), CMS-Flux Ocean v3 (ocean), CMEMS-LSCE (ocean) and the Global Carbon Project (ocean).

The FLUXCOM RS product estimates global terrestrial carbon fluxes by applying multiple machine learning algorithms, including Multivariate Adaptive Regression Splines (MARS), to satellite-based remote sensing inputs. As the FLUXCOM dataset is available only through 2018, while the other products extend to 2019, the comparison for FLUXCOM is limited to that period. GCAS2021 (Jiang et al., 2022) provides a NEE product derived from GOSAT XCO_2 retrievals using the Global Carbon Assimilation System (GCAS), an inverse modeling framework that shares a satellite-based foundation with this study. The TRENDY (Trends in net land–atmosphere carbon exchange) project is a multi-model ensemble (bottom-up framework) designed to assess long-term trends in global terrestrial carbon fluxes. It integrates multiple Earth system and dynamic global vegetation models driven by common input datasets, including atmospheric CO_2 concentration, meteorological forcing, and land-use changes (Friedlingstein, 2020; Sitch et al., 2008). In this study, we used an ensemble of eight models—CABLE-POP, CARDAMOM, CLASSIC, DLEM, EDv3, IBIS, OCN, and YIBS—all of which simulate the full carbon cycle processes encompassing photosynthesis, respiration, carbon storage, and land-use change. For the ocean domain, the CMS-Flux Ocean v3 product (Bowman, 2024) represents a posterior estimate generated under NASA's Carbon Monitoring System

https://doi.org/10.5194/egusphere-2025-5971
Preprint. Discussion started: 19 January 2026

(CMS), combining GOSAT and OCO-2 observations with an atmospheric transport model to infer global air–sea CO_2 exchange. In contrast, the CMEMS-LSCE product (Chau et al., 2022, 2023) reconstructs monthly air–sea CO_2 fluxes and surface pCO_2 fields at 0.25° spatial resolution through an ensemble-based approach integrating satellite observations, in situ measurements, and statistical models. The multi-model mean of ten ocean models participating in the Global Carbon Project—ACCESS, CESM, CNRM, FESOM, IPSL, MOM, MPIOM, MRI, NEMO, and NORESM—was also used for comparison. These models simulate large-scale ocean circulation and biogeochemical carbon processes that govern global air–sea CO_2 exchange, serving as key components of the Global Carbon Budget ocean flux ensemble.

As shown in Figure 5a, our posterior estimates consistently indicate enhanced terrestrial carbon uptake relative to the prior and are comparable to other top-down products (FLUXCOM and GCAS) as well as the bottom-up ensemble (TRENDY). The posterior results show closer agreement with these datasets than the prior does. However, in 2016, although the posterior estimates remain closer to the other products than the prior, a slight discrepancy persists, likely due to the nearly neutral prior flux that year. Over the ocean, the posterior estimates show a comparable magnitude of carbon uptake to both the prior and alternative products (Figure 5b). Although the posterior mean suggests a marginally stronger sink, the difference lies within the uncertainty range and is therefore not statistically significant. This result remains consistent with the bottom-up ensemble (Global Carbon Budget Ocean).

The ocean remains a region of limited observational coverage, where variability in data availability and input types can lead to differences among products. The Northwest Pacific, our primary ocean focus region, is particularly characterized by complex coastal geometries and sparse surface pCO_2 observations, thereby contributing to elevated uncertainties and product-level discrepancies (Wu et al., 2025). Further contributing factors include differences in observational datasets and model configurations. CMS utilizes GOSAT v7.3 and OCO-2 data, whereas CMEMS relies primarily on in situ measurements. GCAS2021 also uses the GOSAT v9r retrievals employed in this study, but differs by adopting CT2019B as the prior flux and MOZART-4 as the transport model instead of GEOS-Chem. These differences likely contribute to the discrepancies observed in the posterior flux estimates.

https://doi.org/10.5194/egusphere-2025-5971
Preprint. Discussion started: 19 January 2026

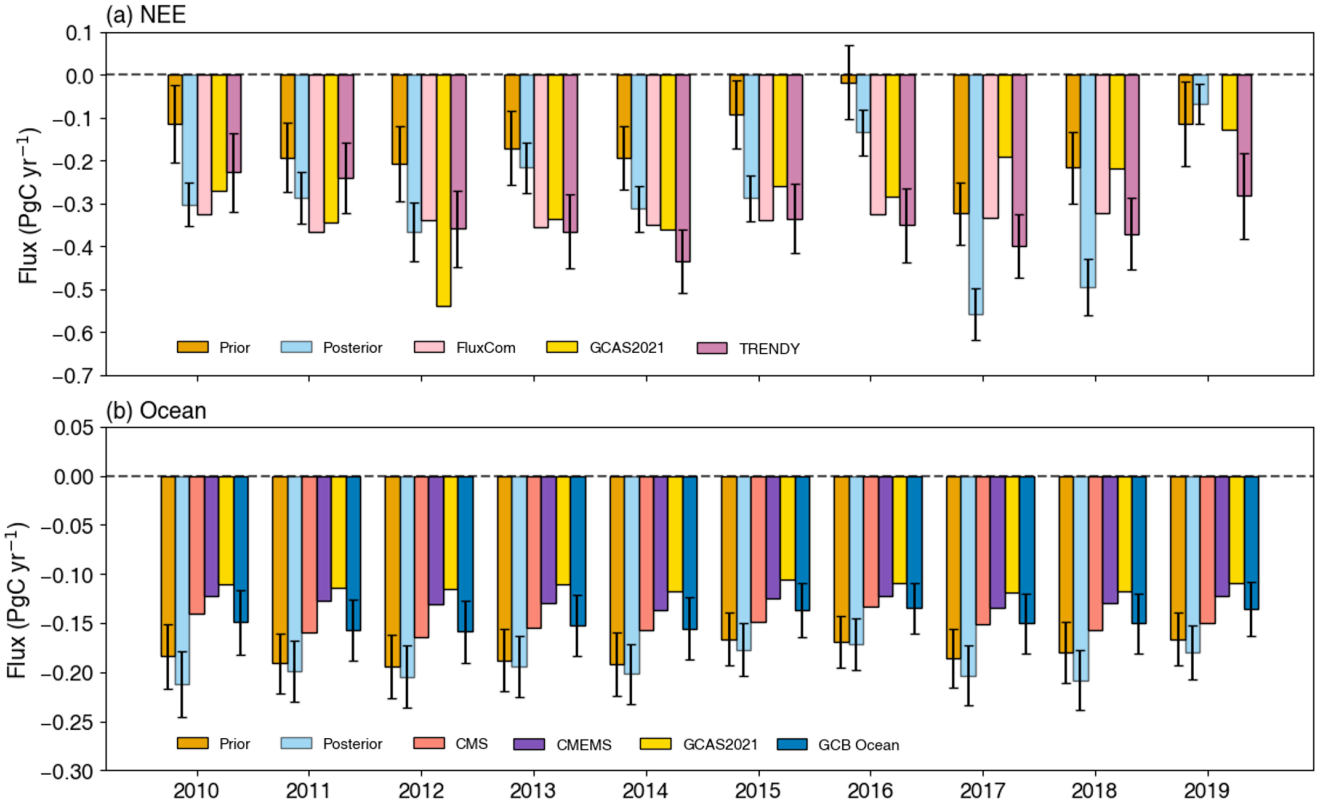

Figure 5. Comparison of prior and posterior flux estimates with other flux products from 2010 to 2019. (a) NEE and (b) Ocean carbon flux over East Asia. Bars indicate annual mean fluxes from each dataset. Error bars represent the uncertainty ranges for the prior and posterior estimates, while those for TRENDY and GCB Ocean denote the inter-model standard deviations.

6 East Asia Carbon Budget (2010–2019)

The carbon budget of East Asia for 2010–2019, incorporating the sink estimated in this study, is summarized as follows (Figure 6). Fossil fuel and biomass burning emissions are derived from ODIAC and GFED4, respectively. Fossil fuel emissions amount to 3.86 PgC yr^{-1}. Compared with the global total fossil fuel emissions of 9.6 PgC yr^{-1} (Friedlingstein, 2020), East Asia accounts for about 40% of the global fossil carbon release.

Biomass burning contributes 0.11 PgC yr^{-1}, while the regional NEE and ocean uptake are −0.31 PgC yr^{-1} and −0.21 PgC yr^{-1}, respectively. These yield a combined sink of −0.52 PgC yr^{-1}, offsetting only 13.6% of fossil fuel emissions. Consequently, the residual carbon that is not compensated by natural sinks accumulates in the atmosphere, leading to an increase in atmospheric CO_2 concentrations. This imbalance between emissions and sinks explains the persistently high atmospheric CO_2 levels

https://doi.org/10.5194/egusphere-2025-5971
Preprint. Discussion started: 19 January 2026

observed over East Asia (Yeh et al., 2023). The atmospheric carbon stock over East Asia is estimated at 38.97 PgC, representing the amount of CO_2 currently retained within the regional atmosphere.

In our East Asia domain, the net surface flux (fossil fuel + biomass burning + NEE + ocean uptake, with NEE and ocean uptake typically negative) is +3.45 PgC yr^{-1} for 2010–2019, indicating a strong net source to the atmosphere. Over the same period, the vertically integrated atmospheric carbon mass within the domain increases at a mean rate of ~0.24 PgC yr^{-1}, implying that only about 7% of the emitted carbon remains stored locally in the atmospheric column. The remaining ~3.21 PgC yr^{-1}, ~93% of the net source, is exported out of the domain by large-scale transport. Most of the carbon emitted from East Asia is transported beyond the regional boundaries. Therefore, East Asian emissions are not confined to a local issue but are linked to downstream transport influencing other regions.

Despite gradual increases in NEE and ocean uptake due to fertilization effects and enhanced solubility associated with pCO_2 gradients, East Asia remains dominated by large fossil fuel emissions. Given this limited natural sink capacity, achieving carbon neutrality will require substantial reductions in fossil fuel use and the enhancement of anthropogenic removals, such as carbon capture and storage (CCS).

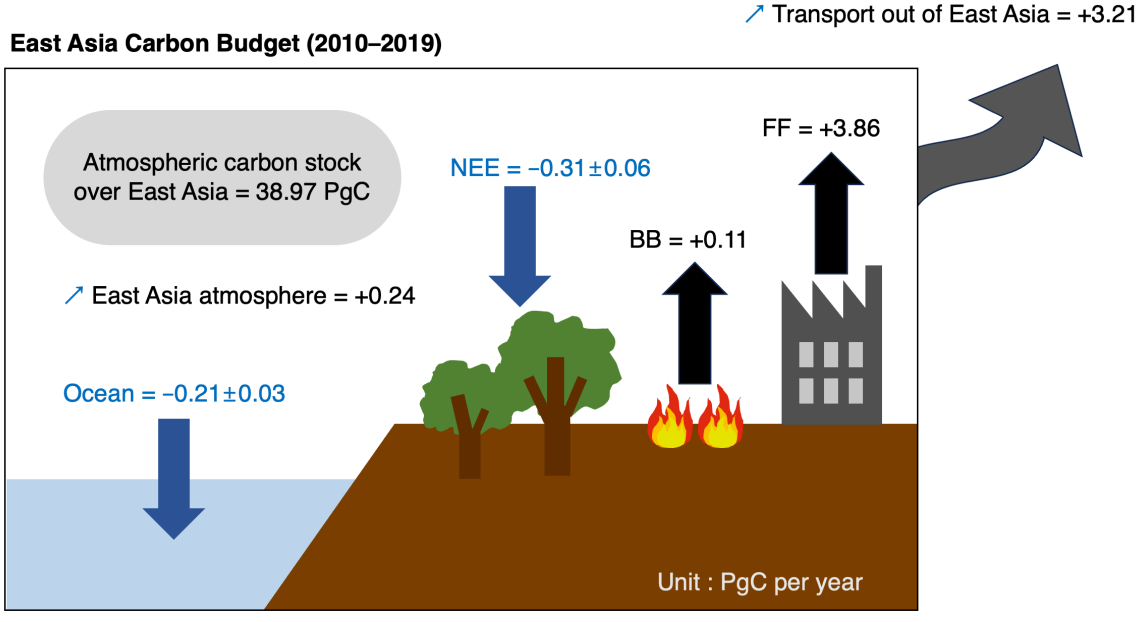

Figure 6. Schematic diagram of the East Asia carbon budget averaged for 2010–2019 (18.5° N–54° N, 73° E–146° E). The atmospheric carbon stock over East Asia, estimated at 38.97 PgC, represents the amount of CO_2 retained within the regional atmosphere. All other fluxes are expressed in PgC yr^{-1} (FF = fossil fuel combustion; BB = biomass burning; NEE = net ecosystem exchange). Downward blue arrows represent CO_2 uptake by the terrestrial and ocean, whereas upward black arrows indicate emissions from biomass burning and fossil fuel combustion.

https://doi.org/10.5194/egusphere-2025-5971
Preprint. Discussion started: 19 January 2026

7. Summary and conclusions

This study provides a top-down estimate of regional carbon fluxes across East Asia (18.5°N–54°N, 73°E–146°E) for the period 2010–2019, using a Bayesian inversion framework constrained by GOSAT ACOS v9.0 XCO_2 retrievals. By applying the GEOS-Chem chemical transport model and incorporating region-specific prior uncertainties based on the standard deviation of terrestrial and ocean carbon fluxes, we optimized both terrestrial and oceanic fluxes. The posterior estimates indicate enhanced carbon uptake compared to the prior, with mean terrestrial NEE ranging from –0.17 to –0.31 PgC yr^{-1} while oceanic uptake changed slightly from –0.20 to –0.21 PgC yr^{-1}, showing no statistically significant difference.

Evaluation against independent surface-based CO_2 observations (WDCGG and TCCON) showed consistent improvements across most stations in terms of correlation, RMSE, and bias, supporting the robustness of the inversion framework. Uncertainty reduction (UR) was generally more substantial over continental regions such as China, whereas smaller or oceanic regions showed limited improvements due to observational constraints.

At the regional scale, most regions acted as persistent carbon sinks throughout the decade, with interannual variability influenced by climate events. Notably, the 2015–2016 Super El Niño was associated with temporary flux reversals, primarily over several regions in China. These reversals were largely driven by ENSO-induced floods and droughts, which suppressed vegetation photosynthetic activity and, in some regions, led to near-neutral or even positive NEE values, indicating temporary carbon release. This suggests that terrestrial carbon sinks can be substantially weakened not only by natural climatic variability such as ENSO, but also by extreme weather events intensified under climate change. An increasing trend in the Enhanced Vegetation Index (EVI), along with improved correlations between EVI and posterior carbon uptake, further supports the credibility of the flux estimates. However, regions dominated by broadleaf forests exhibited persistent negative correlations, likely due to self-shading effects of dense canopies.

Comparison with other top-down and bottom-up flux products showed general agreement in both trend and magnitude. Nonetheless, discrepancies remain, largely due to differences in observational inputs, modeling frameworks, and prior flux assumptions. In particular, oceanic uptake estimates tend to diverge more than terrestrial ones, as ocean regions are more sparsely observed and often include complex coastal zones (Wu et al., 2025).

Although the optimized posterior fluxes indicate enhanced carbon uptake compared to the prior, the East Asian domain remains highly fossil-fuel-dominant. Approximately 7% of the residual carbon accumulates within the regional atmosphere, while the remaining 93% is transported out of the domain by large-scale circulation. Considering the limited capacity of natural carbon sinks, new strategies will be required to mitigate both the persistently high atmospheric CO_2 concentrations over East Asia and the downstream transport of these emissions to other regions.

Overall, this study estimates carbon sinks over East Asia by incorporating region-specific uncertainties and demonstrate the effective use of satellite constraints and a chemical transport model in inverse modeling. The results were evaluated against independent observations and compared with other flux products, while the interannual variability was interpreted through ENSO and vegetation indices. However, the relatively limited observational coverage over ocean regions

https://doi.org/10.5194/egusphere-2025-5971
Preprint. Discussion started: 19 January 2026

resulted in smaller uncertainty reductions, highlighting the need for denser and more continuous oceanic CO_2 observations to further constrain regional flux estimates. Despite this limitation, this study provides valuable insights into the East Asian carbon cycle, which is critical for carbon management, and can support policy strategies aimed at mitigating climate change.

https://doi.org/10.5194/egusphere-2025-5971
Preprint. Discussion started: 19 January 2026

Data availability

The GOSAT ACOS v9.0 XCO_2 retrievals are publicly available from the NASA GES DISC (https://disc.gsfc.nasa.gov; Taylor et al., 2022). Ground-based CO_2 observations are available from the World Data Centre for Greenhouse Gases (WDCGG; https://gaw.kishou.go.jp/). The TCCON (Total Carbon Column Observing Network) data used in this study are publicly available at https://tccondata.org/. The MODIS/Terra EVI data (MOD13C2 Version 6.1) were obtained from the NASA Land Processes Distributed Active Archive Center (LP DAAC), USGS/Earth Resources Observation and Science Center (https://lpdaac.usgs.gov/). The TRENDY model simulation result and Ocean flux products from the Global Carbon Budget 2023 are available via the ICOS Carbon Portal as part of the Global Carbon Budget open data. (https://mdosullivan.github.io/GCB/) The GCAS2021 data are available at https://doi.org/10.5281/zenodo.5829774 (Jiang, 2022). The FLUXCOM data are publicly available for download (CC BY 4.0 license) from the Max Planck Institute for Biogeochemistry (MPI-BGC) data portal after registration (https://www.fluxcom.org). The CMS-Flux Ocean v3 posterior flux product is available from the NASA Goddard Earth Sciences Data and Information Services Center (GES DISC; DOI: 10.5067/9H6GCQKP28AI). The CMEMS-LSCE ocean carbon product is available from the Copernicus Marine Environment Monitoring Service (DOI: 10.48670/moi-00047).

Author contributions

RJP designed the study. MK analyzed the data and wrote the manuscript. JJ supported the data analysis. SIO contributed to the discussion. ESH provided the code used in this study. JIJ and SWY provided valuable comments and advice.

Competing interests

The authors declare that they have no conflict of interest.

Acknowledgements

We acknowledge the data providers of GOSAT, WDCGG, TCCON, TRENDY, Global Carbon Project and other sources used in this study. We thank the developers of the GEOS-Chem model and the global carbon flux products for making their data publicly available.

Financial support

This research has been supported by the Research Program for the Carbon Cycle between Oceans, Land, and Atmosphere of the National Research Foundation (NRF), funded by the Ministry of Science and ICT (2021M3I6A1086803).

https://doi.org/10.5194/egusphere-2025-5971
Preprint. Discussion started: 19 January 2026

References

Baker, D. F., Law, R. M., Gurney, K. R., Rayner, P., Peylin, P., Denning, A. S., Bousquet, P., Bruhwiler, L., Chen, Y. H., Ciais, P., Fung, I. Y., Heimann, M., John, J., Maki, T., Maksyutov, S., Masarie, K., Prather, M., Pak, B., Taguchi, S., and Zhu, Z.: TransCom 3 inversion intercomparison: Impact of transport model errors on the interannual variability of regional CO2 fluxes, 1988-2003, Global Biogeochem Cycles, 20, https://doi.org/10.1029/2004GB002439, 2006.

Bastos, A., Friedlingstein, P., Sitch, S., Chen, C., Mialon, A., Wigneron, J. P., Arora, V. K., Briggs, P. R., Canadell, J. G., Ciais, P., Chevallier, F., Cheng, L., Delire, C., Haverd, V., Jain, A. K., Joos, F., Kato, E., Lienert, S., Lombardozzi, D., Melton, J. R., Myneni, R., Nabel, J. E. M. S., Pongratz, J., Poulter, B., Rödenbeck, C., Séférian, R., Tian, H., Van Eck, C., Viovy, N., Vuichard, N., Walker, A. P., Wiltshire, A., Yang, J., Zaehle, S., Zeng, N., and Zhu, D.: Impact of the 2015/2016 El Niño on the terrestrial carbon cycle constrained by bottom-up and top-down approaches, Philosophical Transactions of the Royal Society B: Biological Sciences, 373, https://doi.org/10.1098/rstb.2017.0304, 2018.

Basu, S., Baker, D. F., Chevallier, F., Patra, P. K., Liu, J., and Miller, J. B.: The impact of transport model differences on CO2 surface flux estimates from OCO-2 retrievals of column average CO2, Atmos Chem Phys, 18, 7189–7215, https://doi.org/10.5194/acp-18-7189-2018, 2018.

Bowman, K.: Carbon Monitoring System Carbon Flux Ocean Prior L4 V3, Greenbelt, MD, 2024.

Byrne, B., Jones, D. B. A., Strong, K., Polavarapu, S. M., Harper, A. B., Baker, D. F., and Maksyutov, S.: On what scales can GOSAT flux inversions constrain anomalies in terrestrial ecosystems?, Atmos Chem Phys, 19, 13017–13035, https://doi.org/10.5194/acp-19-13017-2019, 2019.

Chau, T. T. T., Gehlen, M., and Chevallier, F.: A seamless ensemble-based reconstruction of surface ocean pCO2 and air-sea CO2 fluxes over the global coastal and open oceans, Biogeosciences, 19, 1087–1109, https://doi.org/10.5194/bg-19-1087-2022, 2022.

Chau, T. T. T., Gehlen, M., Metzl, N., and Chevallier, F.: CMEMS-LSCE: A global 0.25-degree, monthly reconstruction of the surface ocean carbonate system , 2023.

Chevallier, F., Remaud, M., O'Dell, C. W., Baker, D., Peylin, P., and Cozic, A.: Objective evaluation of surface- and satellite-driven carbon dioxide atmospheric inversions, Atmos Chem Phys, 19, 14233–14251, https://doi.org/10.5194/acp-19-14233-2019, 2019.

Connor, B. J., Boesch, H., Toon, G., Sen, B., Miller, C., and Crisp, D.: Orbiting Carbon Observatory: Inverse method and prospective error analysis, Journal of Geophysical Research Atmospheres, 113, https://doi.org/10.1029/2006JD008336, 2008.

Cox, P. M., Pearson, D., Booth, B. B., Friedlingstein, P., Huntingford, C., Jones, C. D., and Luke, C. M.: Sensitivity of tropical carbon to climate change constrained by carbon dioxide variability, Nature, 494, 341–344, https://doi.org/10.1038/nature11882, 2013.

Deng, F. and Chen, J. M.: Recent global CO 2 flux inferred from atmospheric CO 2 observations and its regional analyses, Biogeosciences, 8, 3263–3281, https://doi.org/10.5194/bg-8-3263-2011, 2011.

https://doi.org/10.5194/egusphere-2025-5971
Preprint. Discussion started: 19 January 2026

Deng, F., Chen, J. M., Ishizawa, M., Yuen, C. W., Mo, G., Higuchi, K., Chan, D., and Maksyutov, S.: Global monthly CO2 flux inversion with a focus over North America, in: Tellus, Series B: Chemical and Physical Meteorology, 179–190, https://doi.org/10.1111/j.1600-0889.2006.00235.x, 2007.

Deng, F., Jones, D. B. A., Henze, D. K., Bousserez, N., Bowman, K. W., Fisher, J. B., Nassar, R., O'Dell, C., Wunch, D., Wennberg, P. O., Kort, E. A., Wofsy, S. C., Blumenstock, T., Deutscher, N. M., Griffith, D. W. T., Hase, F., Heikkinen, P., Sherlock, V., Strong, K., Sussmann, R., and Warneke, T.: Inferring regional sources and sinks of atmospheric CO2 from GOSAT XCO2 data, Atmos Chem Phys, 14, 3703–3727, https://doi.org/10.5194/acp-14-3703-2014, 2014.

Fang, Y., Michalak, A. M., Schwalm, C. R., Huntzinger, D. N., Berry, J. A., Ciais, P., Piao, S., Poulter, B., Fisher, J. B., Cook, R. B., Hayes, D., Huang, M., Ito, A., Jain, A., Lei, H., Lu, C., Mao, J., Parazoo, N. C., Peng, S., Ricciuto, D. M., Shi, X., Tao, B., Tian, H., Wang, W., Wei, Y., and Yang, J.: Global land carbon sink response to temperature and precipitation varies with ENSO phase, Environmental Research Letters, 12, https://doi.org/10.1088/1748-9326/aa6e8e, 2017.

Feng, S., Jiang, F., Wu, Z., Wang, H., Ju, W., and Wang, H.: CO Emissions Inferred From Surface CO Observations Over China in December 2013 and 2017, Journal of Geophysical Research: Atmospheres, 125, https://doi.org/10.1029/2019JD031808, 2020.

Friedlingstein, P.: Global carbon budget 2020, Earth Syst Sci Data, 12, https://doi.org/10.5194/essd-12-3269-2020, 2020.

Friedlingstein, P., O'Sullivan, M., Jones, M. W., Andrew, R. M., Bakker, D. C. E., Hauck, J., Landschützer, P., Le Quéré, C., Luijkx, I. T., Peters, G. P., Peters, W., Pongratz, J., Schwingshackl, C., Sitch, S., Canadell, J. G., Ciais, P., Jackson, R. B., Alin, S. R., Anthoni, P., Barbero, L., Bates, N. R., Becker, M., Bellouin, N., Decharme, B., Bopp, L., Brasika, I. B. M., Cadule, P., Chamberlain, M. A., Chandra, N., Chau, T. T. T., Chevallier, F., Chini, L. P., Cronin, M., Dou, X., Enyo, K., Evans, W., Falk, S., Feely, R. A., Feng, L., Ford, D. J., Gasser, T., Ghattas, J., Gkritzalis, T., Grassi, G., Gregor, L., Gruber, N., Gürses, Ö., Harris, I., Hefner, M., Heinke, J., Houghton, R. A., Hurtt, G. C., Iida, Y., Ilyina, T., Jacobson, A. R., Jain, A., Jarníková, T., Jersild, A., Jiang, F., Jin, Z., Joos, F., Kato, E., Keeling, R. F., Kennedy, D., Goldewijk, K. K., Knauer, J., Korsbakken, J. I., Körtzinger, A., Lan, X., Lefèvre, N., Li, H., Liu, J., Liu, Z., Ma, L., Marland, G., Mayot, N., McGuire, P. C., McKinley, G. A., Meyer, G., Morgan, E. J., Munro, D. R., Nakaoka, S. I., Niwa, Y., O'Brien, K. M., Olsen, A., Omar, A. M., Ono, T., Paulsen, M., Pierrot, D., Pocock, K., Poulter, B., Powis, C. M., Rehder, G., Resplandy, L., Robertson, E., Rödenbeck, C., Rosan, T. M., Schwinger, J., Séférian, R., et al.: Global Carbon Budget 2023, Earth Syst Sci Data, 15, 5301–5369, https://doi.org/10.5194/essd-15-5301-2023, 2023.

Gerbig, C., Lin, J. C., Wofsy, S. C., Daube, B. C., Andrews, A. E., Stephens, B. B., Bakwin, P. S., and Grainger, C. A.: Toward constraining regional-scale fluxes of CO2 with atmospheric observations over a continent: 2. Analysis of COBRA data using a receptor-oriented framework, Journal of Geophysical Research: Atmospheres, 108, https://doi.org/10.1029/2003jd003770, 2003.

Gilfillan, D. and Marland, G.: CDIAC-FF: Global and national CO2 emissions from fossil fuel combustion and cement manufacture: 1751-2017, Earth Syst Sci Data, 13, 1667–1680, https://doi.org/10.5194/essd-13-1667-2021, 2021.

https://doi.org/10.5194/egusphere-2025-5971
Preprint. Discussion started: 19 January 2026

Gurney, K. R., Law, R. M., Denning, A. S., Rayner, P. J., Baker, D., Bousquet, P., Bruhwiler, L., Chen, Y.-H., Ciais, P., Fan, S., Fung, I. Y., Gloor, M., Heimann, M., Higuchi, K., John, J., Maki, T., Maksyutov, S., Masarie, K., Peylin, P., Prather, M., Pak, B. C., Randerson, J., Sarmiento, J., Taguchi, S., Takahashi, T., and Yuen, C.-W.: Towards robust regional estimates of CO2 sources and sinks using atmospheric transport models, Nature, 415, 626–630, https://doi.org/10.1038/415626a, 2002.

Gurney, K. R., Law, R. M., Denning, A. S., Rayner, P. J., Baker, D., Bousquet, P., Bruhwiler, L., Chen, Y.-H., Ciais, P., Fan, S., Fung, I. Y., Gloor, M., Heimann, M., Higuchi, K., John, J., Kowalczyk, E., Maki, T., Maksyutov, S., Peylin, P., Prather, M., Pak, B. C., Sarmiento, J., Taguchi, S., Takahashi, T., and Yuen, C.-W.: TransCom 3 CO 2 inversion intercomparison: 1. Annual mean control results and sensitivity to transport and prior flux information, 55, 555–579, 2003.

Houweling, S., Baker, D., Basu, S., Boesch, H., Butz, A., Chevallier, F., Deng, F., Dlugokencky, E. J., Feng, L., Ganshin, A., Hasekamp, O., Jones, D., Maksyutov, S., Marshall, J., Oda, T., O'Dell, C. W., Oshchepkov, S., Palmer, P. I., Peylin, P., Poussi, Z., Reum, F., Takagi, H., Yoshida, Y., and Zhuravlev, R.: An intercomparison of inversemodels for estimating sources and sinks of CO2 using GOSAT measurements, J Geophys Res, 120, 5253–5266, https://doi.org/10.1002/2014JD022962, 2015.

Intergovernmental Panel on Climate Change (IPCC): Global Carbon and Other Biogeochemical Cycles and Feedbacks, in: Climate Change 2021 – The Physical Science Basis, Cambridge University Press, 673–816, https://doi.org/10.1017/9781009157896.007, 2023.

Jiang, F., Wang, H. W., Chen, J. M., Zhou, L. X., Ju, W. M., Ding, A. J., Liu, L. X., and Peters, W.: Nested atmospheric inversion for the terrestrial carbon sources and sinks in China, Biogeosciences, 10, 5311–5324, https://doi.org/10.5194/bg-10-5311-2013, 2013a.

Jiang, F., Wang, H. W., Chen, J. M., Zhou, L. X., Ju, W. M., Ding, A. J., Liu, L. X., and Peters, W.: Nested atmospheric inversion for the terrestrial carbon sources and sinks in China, Biogeosciences, 10, 5311–5324, https://doi.org/10.5194/bg-10-5311-2013, 2013b.

Jiang, F., Wang, H., Chen, J. M., Ju, W., Tian, X., Feng, S., Li, G., Chen, Z., Zhang, S., Lu, X., Liu, J., Wang, H., Wang, J., He, W., and Wu, M.: Regional CO2 fluxes from 2010 to 2015 inferred from GOSAT XCO2 retrievals using a new version of the Global Carbon Assimilation System, Atmos Chem Phys, 21, 1963–1985, https://doi.org/10.5194/acp-21-1963-2021, 2021.

Jiang, F., Ju, W., He, W., Wu, M., Wang, H., Wang, J., Jia, M., Feng, S., Zhang, L., and Chen, J. M.: A 10-year global monthly averaged terrestrial net ecosystem exchange dataset inferred from the ACOS GOSAT v9 XCO2retrievals (GCAS2021), Earth Syst Sci Data, 14, 3013–3037, https://doi.org/10.5194/essd-14-3013-2022, 2022a.

Jiang, P., Ding, W., Yuan, Y., Ye, W., and Mu, Y.: Interannual variability of vegetation sensitivity to climate in China, J Environ Manage, 301, https://doi.org/10.1016/j.jenvman.2021.113768, 2022b.

Jin, J., Lin, H. X., Heemink, A., and Segers, A.: Spatially varying parameter estimation for dust emissions using reduced-tangent-linearization 4DVar, Atmos Environ, 187, 358–373, https://doi.org/10.1016/j.atmosenv.2018.05.060, 2018.

Joos, F. and Spahni, R.: Rates of change in natural and anthropogenic radiative forcing over the past 20,000 years, 2008.

Jung, M., Schwalm, C., Migliavacca, M., Walther, S., Camps-Valls, G., Koirala, S., Anthoni, P., Besnard, S., Bodesheim, P., Carvalhais, N., Chevallier, F., Gans, F., S Goll, D., Haverd, V., Köhler, P., Ichii, K., K Jain, A., Liu, J., Lombardozzi, D., E

https://doi.org/10.5194/egusphere-2025-5971
Preprint. Discussion started: 19 January 2026

M S Nabel, J., A Nelson, J., O'Sullivan, M., Pallandt, M., Papale, D., Peters, W., Pongratz, J., Rödenbeck, C., Sitch, S., Tramontana, G., Walker, A., Weber, U., and Reichstein, M.: Scaling carbon fluxes from eddy covariance sites to globe: Synthesis and evaluation of the FLUXCOM approach, Biogeosciences, 17, 1343–1365, https://doi.org/10.5194/bg-17-1343-2020, 2020.

Kaminski, T., Scholze, M., and Houweling, S.: Quantifying the benefit of A-SCOPE data for reducing uncertainties in terrestrial carbon fluxes in CCDAS, Tellus B Chem Phys Meteorol, 62, 784–796, https://doi.org/10.1111/j.1600-0889.2010.00483.x, 2010.

Kondo, M., Patra, P. K., Sitch, S., Friedlingstein, P., Poulter, B., Chevallier, F., Ciais, P., Canadell, J. G., Bastos, A., Lauerwald, R., Calle, L., Ichii, K., Anthoni, P., Arneth, A., Haverd, V., Jain, A. K., Kato, E., Kautz, M., Law, R. M., Lienert, S., Lombardozzi, D., Maki, T., Nakamura, T., Peylin, P., Rödenbeck, C., Zhuravlev, R., Saeki, T., Tian, H., Zhu, D., and Ziehn, T.: State of the science in reconciling top-down and bottom-up approaches for terrestrial CO2 budget, Glob Chang Biol, 26, 1068–1084, https://doi.org/10.1111/gcb.14917, 2020.

Kou, X., Peng, Z., Zhang, M., Hu, F., Han, X., Li, Z., and Lei, L.: The carbon sink in China as seen from GOSAT with a regional inversion system based on the Community Multi-scale Air Quality (CMAQ) and ensemble Kalman smoother (EnKS), Atmos Chem Phys, 23, 6719–6741, https://doi.org/10.5194/acp-23-6719-2023, 2023.

Kulawik, S. S., Crowell, S., Baker, D., Liu, J., McKain, K., Sweeney, C., Biraud, S. C., Wofsy, S., O'Dell, C. W., Wennberg, P. O., Wunch, D., Roehl, C. M., Deutscher, N. M., Kiel, M., Griffith, D. W. T., Velazco, V. A., Notholt, J., Warneke, T., Petri, C., De Mazière, M., Sha, M. K., Sussmann, R., Rettinger, M., Pollard, D. F., Morino, I., Uchino, O., Hase, F., Feist, D. G., Roche, S., Strong, K., Kivi, R., Iraci, L., Shiomi, K., Dubey, M. K., Sepulveda, E., Rodriguez, O. E. G., Té, Y., Jeseck, P., Heikkinen, P., Dlugokencky, E. J., Gunson, M. R., Eldering, A., Crisp, D., Fisher, B., and Osterman, G. B.: Characterization of OCO-2 and ACOS-GOSAT biases and errors for CO2 flux estimates, https://doi.org/10.5194/amt-2019-257, 28 October 2019.

Lan, X., Tans, P., and K.W. Thoning: Trends in globally-averaged CO2 determined from NOAA Global Monitoring Laboratory measurements. Version Thursday, 05-Jun-2025 08:00:43 MDT, 2025.

Liu, J., Baskaran, L., Bowman, K., Schimel, D., Anthony Bloom, A., Parazoo, C. N., Oda, T., Carroll, D., Menemenlis, D., Joiner, J., Commane, R., Daube, B., Gatti, V. L., McKain, K., Miller, J., Stephens, B. B., Sweeney, C., and Wofsy, S.: Carbon Monitoring System Flux Net Biosphere Exchange 2020 (CMS-Flux NBE 2020), Earth Syst Sci Data, 13, 299–330, https://doi.org/10.5194/essd-13-299-2021, 2021.

Liu, Y., Zhao, Y., Wu, W., Ao, X., and Chen, R.: The Response of Vegetation Dynamics to Climate in Xinjiang from 1991 to 2018, Forests, 15, https://doi.org/10.3390/f15122065, 2024.

Lu, B., Li, H., Wu, J., Zhang, T., Liu, J., Liu, B., Chen, Y., and Baishan, J.: Impact of El Niño and Southern Oscillation on the summer precipitation over Northwest China, Atmospheric Science Letters, 20, https://doi.org/10.1002/asl.928, 2019.

Ma, F., Ye, A., You, J., and Duan, Q.: 2015–16 floods and droughts in China, and its response to the strong El Niño, Science of the Total Environment, 627, 1473–1484, https://doi.org/10.1016/j.scitotenv.2018.01.280, 2018.

https://doi.org/10.5194/egusphere-2025-5971
Preprint. Discussion started: 19 January 2026

Monteil, G., Broquet, G., Scholze, M., Lang, M., Karstens, U., Gerbig, C., Koch, F. T., Smith, N. E., Thompson, R. L., Luijkx, I. T., White, E., Meesters, A., Ciais, P., Ganesan, A. L., Manning, A., Mischurow, M., Peters, W., Peylin, P., Tarniewicz, J., Rigby, M., Rödenbeck, C., Vermeulen, A., and Walton, E. M.: The regional European atmospheric transport inversion comparison, EUROCOM: First results on European-wide terrestrial carbon fluxes for the period 2006-2015, Atmos Chem Phys, 20, 12063–12091, https://doi.org/10.5194/acp-20-12063-2020, 2020.

Nassar, R., Jones, D. B. A., Suntharalingam, P., Chen, J. M., Andres, R. J., Wecht, K. J., Yantosca, R. M., Kulawik, S. S., Bowman, K. W., Worden, J. R., MacHida, T., and Matsueda, H.: Modeling global atmospheric CO2 with improved emission inventories and CO2 production from the oxidation of other carbon species, Geosci Model Dev, 3, 689–716, https://doi.org/10.5194/gmd-3-689-2010, 2010.

Nassar, R., Jones, D. B. A., Kulawik, S. S., Worden, J. R., Bowman, K. W., Andres, R. J., Suntharalingam, P., Chen, J. M., Brenninkmeijer, C. A. M., Schuck, T. J., Conway, T. J., and Worthy, D. E.: Inverse modeling of CO2 sources and sinks using satellite observations of CO2 from TES and surface flask measurements, Atmos Chem Phys, 11, 6029–6047, https://doi.org/10.5194/acp-11-6029-2011, 2011.

Nassar, R., Napier-Linton, L., Gurney, K. R., Andres, R. J., Oda, T., Vogel, F. R., and Deng, F.: Improving the temporal and spatial distribution of co2 emissions from global fossil fuel emission data sets, Journal of Geophysical Research Atmospheres, 118, 917–933, https://doi.org/10.1029/2012JD018196, 2013.

Noumonvi, K. D. and Ferlan, M.: Empirical vs. light-use efficiency modelling for estimating carbon fluxes in a mid-succession ecosystem developed on abandoned karst grassland, PLoS One, 15, https://doi.org/10.1371/journal.pone.0237351, 2020.

Oda, T. and Maksyutov, S.: A very high-resolution (1km×1 km) global fossil fuel CO2 emission inventory derived using a point source database and satellite observations of nighttime lights, Atmos Chem Phys, 11, 543–556, https://doi.org/10.5194/acp-11-543-2011, 2011.

Oda, T., Maksyutov, S., and Andres, R. J.: The Open-source Data Inventory for Anthropogenic CO2, version 2016 (ODIAC2016): A global monthly fossil fuel CO2 gridded emissions data product for tracer transport simulations and surface flux inversions, Earth Syst Sci Data, 10, 87–107, https://doi.org/10.5194/essd-10-87-2018, 2018.

Palmer, P. I., Jacob, D. J., Jones, D. B. A., Heald, C. L., Yantosca, R. M., Logan, J. A., Sachse, G. W., and Streets, D. G.: Inverting for emissions of carbon monoxide from Asia using aircraft observations over the western Pacific, Journal of Geophysical Research: Atmospheres, 108, https://doi.org/10.1029/2003jd003397, 2003.

Panmao, Z., Rong, Y. U., Yanjun, G., Li, Q., Xuejuan, R., Wang, Y., Liu, Y., and Yihui, D.: The Strong El Niño of 2015/16 and Its Dominant Impacts on Global and China's Climate, J. Meteor. Res, 30, 283–297, https://doi.org/10.1007/s13, n.d.

Peters, W., Jacobson, A. R., Sweeney, C., Andrews, A. E., Conway, T. J., Masarie, K., Miller, J. B., P Bruhwiler, L. M., Pé tron, G., Hirsch, A. I., J Worthy, D. E., van der Werf, G. R., Randerson, J. T., Wennberg, P. O., Krol, M. C., and Tans, P. P.: An atmospheric perspective on North American carbon dioxide exchange: CarbonTracker, 2007.

https://doi.org/10.5194/egusphere-2025-5971
Preprint. Discussion started: 19 January 2026

Peylin, P., Law, R. M., Gurney, K. R., Chevallier, F., Jacobson, A. R., Maki, T., Niwa, Y., Patra, P. K., Peters, W., Rayner, P. J., Rödenbeck, C., Van Der Laan-Luijkx, I. T., and Zhang, X.: Global atmospheric carbon budget: Results from an ensemble of atmospheric CO2 inversions, Biogeosciences, 10, 6699–6720, https://doi.org/10.5194/bg-10-6699-2013, 2013.

Potithep, S., Nagai, S., Nasahara, K. N., Muraoka, H., and Suzuki, R.: Two separate periods of the LAI-VIs relationships using in situ measurements in a deciduous broadleaf forest, Agric For Meteorol, 169, 148–155, https://doi.org/10.1016/j.agrformet.2012.09.003, 2013.

Randerson, J. T., van der Werf, G. R., Giglio, L., Collatz, G. J., and Kasibhatla, P. S.: Global Fire Emissions Database, Version 4.1 (GFEDv4), 2018.

Ren, H. L., Wang, R., Zhai, P., Ding, Y., and Lu, B.: Upper-ocean dynamical features and prediction of the super El Niño in 2015/16: A comparison with the cases in 1982/83 and 1997/98, Journal of Meteorological Research, 31, 278–294, https://doi.org/10.1007/s13351-017-6194-3, 2017.

Rodgers, C. D.: Inverse methods for atmospheric sounding: theory and practice, World scientific, 2000.

Schourup-Kristensen, V., Wekerle, C., Wolf-Gladrow, D. A., and Völker, C.: Arctic Ocean biogeochemistry in the high resolution FESOM 1.4-REcoM2 model, Prog Oceanogr, 168, 65–81, https://doi.org/10.1016/j.pocean.2018.09.006, 2018.

Sitch, S., Huntingford, C., Gedney, N., Levy, P. E., Lomas, M., Piao, S. L., Betts, R., Ciais, P., Cox, P., Friedlingstein, P., Jones, C. D., Prentice, I. C., and Woodward, F. I.: Evaluation of the terrestrial carbon cycle, future plant geography and climate-carbon cycle feedbacks using five Dynamic Global Vegetation Models (DGVMs), Glob Chang Biol, 14, 2015–2039, https://doi.org/10.1111/j.1365-2486.2008.01626.x, 2008.

Sitch, S., Friedlingstein, P., Gruber, N., Jones, S. D., Murray-Tortarolo, G., Ahlström, A., Doney, S. C., Graven, H., Heinze, C., Huntingford, C., Levis, S., Levy, P. E., Lomas, M., Poulter, B., Viovy, N., Zaehle, S., Zeng, N., Arneth, A., Bonan, G., Bopp, L., Canadell, J. G., Chevallier, F., Ciais, P., Ellis, R., Gloor, M., Peylin, P., Piao, S. L., Le Quéré, C., Smith, B., Zhu, Z., and Myneni, R.: Recent trends and drivers of regional sources and sinks of carbon dioxide, Biogeosciences, 12, 653–679, https://doi.org/10.5194/bg-12-653-2015, 2015.

Suntharalingam, P., Jacob, D. D., Palmer, P. I., Logan, J. A., Yantosca, R. M., Xiao, Y., Evans, M. J., Streets, D. G., Vay, S. L., and Sachse, G. W.: Improved quantificaion of Chinese carbon fluxes using CO2/CO correlations in Asian outflow, Journal of Geophysical Research Atmospheres, 109, https://doi.org/10.1029/2003JD004362, 2004.

Takagi, H., Saeki, T., Oda, T., Saito, M., Valsala, V., Belikov, D., Saito, R., Yoshida, Y., Morino, I., Uchino, O., Andres, R. J., Yokota, T., and Maksyutov, S.: On the benefit of GOSAT observations to the estimation of regional CO2 fluxes, Scientific Online Letters on the Atmosphere, 7, 161–164, https://doi.org/10.2151/sola.2011-041, 2011.

Taylor, T. E., O'Dell, C. W., Crisp, D., Kuze, A., Lindqvist, H., Wennberg, P. O., Chatterjee, A., Gunson, M., Eldering, A., Fisher, B., Kiel, M., Nelson, R. R., Merrelli, A., Osterman, G., Chevallier, F., Palmer, P. I., Feng, L., Deutscher, N. M., Dubey, M. K., Feist, D. G., García, O. E., Griffith, D. W. T., Hase, F., Iraci, L. T., Kivi, R., Liu, C., De Mazière, M., Morino, I., Notholt, J., Oh, Y. S., Ohyama, H., Pollard, D. F., Rettinger, M., Schneider, M., Roehl, C. M., Sha, M. K., Shiomi, K., Strong, K., Sussmann, R., Té, Y., Velazco, V. A., Vrekoussis, M., Warneke, T., and Wunch, D.: An 11-year record of XCO2 estimates

https://doi.org/10.5194/egusphere-2025-5971
Preprint. Discussion started: 19 January 2026

derived from GOSAT measurements using the NASA ACOS version 9 retrieval algorithm, Earth Syst Sci Data, 14, 325–360, https://doi.org/10.5194/essd-14-325-2022, 2022.

Thompson, R. L., Patra, P. K., Chevallier, F., Maksyutov, S., Law, R. M., Ziehn, T., Van Der Laan-Luijkx, I. T., Peters, W., Ganshin, A., Zhuravlev, R., Maki, T., Nakamura, T., Shirai, T., Ishizawa, M., Saeki, T., Machida, T., Poulter, B., Canadell, J. G., and Ciais, P.: Top-down assessment of the Asian carbon budget since the mid 1990s, Nat Commun, 7, https://doi.org/10.1038/ncomms10724, 2016.

Tian, H., Chen, G., Liu, M., Zhang, C., Sun, G., Lu, C., Xu, X., Ren, W., Pan, S., and Chappelka, A.: Model estimates of net primary productivity, evapotranspiration, and water use efficiency in the terrestrial ecosystems of the southern United States during 1895-2007, For Ecol Manage, 259, 1311–1327, https://doi.org/10.1016/j.foreco.2009.10.009, 2010.

Tolk, L. F., Meesters, A. G. C. A., Dolman, A. J., and Peters, W.: Modelling representation errors of atmospheric CO 2 mixing ratios at a regional scale, Atmos. Chem. Phys, 6587–6596 pp., 2008.

UNFCCC: Paris Agreement, 2015.

Wang, H., Jiang, F., Wang, J., Ju, W., and Chen, J. M.: Terrestrial ecosystem carbon flux estimated using GOSAT and OCO-2 XCO2 retrievals, Atmos Chem Phys, 19, 12067–12082, https://doi.org/10.5194/acp-19-12067-2019, 2019.

Wang, J., Feng, L., Palmer, P. I., Liu, Y., Fang, S., Bösch, H., O'Dell, C. W., Tang, X., Yang, D., Liu, L., and Xia, C. Z.: Large Chinese land carbon sink estimated from atmospheric carbon dioxide data, Nature, 586, 720–723, https://doi.org/10.1038/s41586-020-2849-9, 2020.

Wang, W., Ciais, P., Nemani, R. R., Canadell, J. G., Piao, S., Sitch, S., White, M. A., Hashimoto, H., Milesi, C., and Myneni, R. B.: Variations in atmospheric CO2 growth rates coupled with tropical temperature, Proc Natl Acad Sci U S A, 110, 13061–13066, https://doi.org/10.1073/pnas.1219683110, 2013.

Wang, X., Piao, S., Ciais, P., Friedlingstein, P., Myneni, R. B., Cox, P., Heimann, M., Miller, J., Peng, S., Wang, T., Yang, H., and Chen, A.: A two-fold increase of carbon cycle sensitivity to tropical temperature variations, Nature, 506, 212–215, https://doi.org/10.1038/nature12915, 2014.

WMO: Wmo statement on the state of the global climate in 2016, WORLD METEOROLOGICAL ORG, Geneva, 2017.

Wu, Z., Lu, W., Roobaert, A., Song, L., Yan, X.-H., and Cai, W.-J.: A machine-learning reconstruction of sea surface p CO $_2$ in the North American Atlantic Coastal Ocean Margin from 1993 to 2021, Earth Syst Sci Data, 17, 43–63, https://doi.org/10.5194/essd-17-43-2025, 2025.

Wunch, D., Toon, G. C., Blavier, J.-F. L., Washenfelder, R. A., Notholt, J., Connor, B. J., Griffith, D. W. T., Sherlock, V., and Wennberg, P. O.: The Total Carbon Column Observing Network, Philosophical Transactions of the Royal Society A: Mathematical, Physical and Engineering Sciences, 369, 2087–2112, https://doi.org/10.1098/rsta.2010.0240, 2011.

Wunch, D., Wennberg, P. O., Osterman, G., Fisher, B., Naylor, B., Roehl, M. C., O'Dell, C., Mandrake, L., Viatte, C., Kiel, M., Griffith, D. W. T., Deutscher, N. M., Velazco, V. A., Notholt, J., Warneke, T., Petri, C., De Maziere, M., Sha, M. K., Sussmann, R., Rettinger, M., Pollard, D., Robinson, J., Morino, I., Uchino, O., Hase, F., Blumenstock, T., Feist, D. G., Arnold, S. G., Strong, K., Mendonca, J., Kivi, R., Heikkinen, P., Iraci, L., Podolske, J., Hillyard, P., Kawakami, S., Dubey, M. K.,

https://doi.org/10.5194/egusphere-2025-5971
Preprint. Discussion started: 19 January 2026

Parker, H. A., Sepulveda, E., García, O. E., Te, Y., Jeseck, P., Gunson, M. R., Crisp, D., and Eldering, A.: Comparisons of the Orbiting Carbon Observatory-2 (OCO-2) XCO2 measurements with TCCON, https://doi.org/10.5194/amt-10-2209-2017, 13 June 2017.

Yeh, S. W., Shin, M. S., Ma, S. J., Kug, J. S., and Moon, B. K.: Understanding elevated CO2 concentrations in East Asia relative to the global mean during boreal spring on the slow and interannual timescales, Science of the Total Environment, 901, https://doi.org/10.1016/j.scitotenv.2023.166098, 2023.

You, Y., Tian, H., Pan, S., Shi, H., Bian, Z., Gurgel, A., Huang, Y., Kicklighter, D., Liang, X. Z., Lu, C., Melillo, J., Miao, R., Pan, N., Reilly, J., Ren, W., Xu, R., Yang, J., Yu, Q., and Zhang, J.: Incorporating dynamic crop growth processes and management practices into a terrestrial biosphere model for simulating crop production in the United States: Toward a unified modeling framework, Agric For Meteorol, 325, https://doi.org/10.1016/j.agrformet.2022.109144, 2022.

Yue, C., Ciais, P., Bastos, A., Chevallier, F., Yin, Y., Rödenbeck, C., and Park, T.: Vegetation greenness and land carbon-flux anomalies associated with climate variations: A focus on the year 2015, Atmos Chem Phys, 17, 13903–13919, https://doi.org/10.5194/acp-17-13903-2017, 2017.

Zhai, P., Yu, R., Guo, Y., Li, Q., Xuejuan, R., Wang, Y., Liu, Y., and Yihui, D.: The Strong El Niño of 2015/16 and Its Dominant Impacts on Global and China's Climate, J. Meteor. Res, 30, 283–297, https://doi.org/10.1007/s13, 2016.

Zhu, H. and Tan, Y.: The Origin of Evergreen Broad-Leaved Forests in East Asia from the Evidence of Floristic Elements, https://doi.org/10.3390/plants13081106, 1 April 2024.